First steps of the melting of an amorphous polymer through a hot-end of a material extrusion additive manufacturing

Sarah Marion, Lucas Sardo, Thomas Joffre, Franck Pigeonneau

First steps of the melting of an amorphous polymer through a hot-end of a material extrusion additive manufacturing

S. Marion[a,b], L. Sardo[c], T. Joffre[d], F. Pigeonneau[a,*]

[a] *MINES Paris, PSL Research University, CEMEF - Centre for material forming, CNRS UMR 7635, CS 10207, rue Claude Daunesse 06904 Sophia Antipolis Cedex, France*
[b] *Mines Saint-Etienne, Univ Lyon, CNRS, UMR 5307 LGF, Centre SMS, 42023 Saint-Etienne, France*
[c] *Sciences Computers Consultants, 10 rue du plateau des Glières, 42000 Saint-Etienne, France*
[d] *IPC Innovation Plasturgie Composites, 2 rue Pierre & Marie Curie, 01100 Bellignat, France*

Abstract

The melting of an amorphous polymer filament through the hot end of a material extrusion process is addressed using computational multiphase fluid dynamics coupled to heat transfer. Only the flow through the heat block is investigated. The air gap between the filament and the interior of the extruder is accounted for. The polymer/air interface is implicitly tracked by a level-set method. The system of equations is solved using a finite element method with a time-marching method. Three extrusion velocities are investigated. For the lowest velocity, after the contact of the polymer with the extruder on the nozzle, the air gap disappears with time. The transient regime lasts a few tens of seconds. For the two larger velocities, even if the air gap is more and more reduced with time, it persists for a long time. The extension of the air gap increases with the velocity. The feeding force needed to push the filament is obtained by the integration of the tension on the surface of the extruder. After a transient regime driven by the heat transfer, a steady-state regime is observed for the three velocities. Roughly, the feeding force increases linearly with the extrusion velocity. A good agreement is found with experimental results for the two smallest velocities.

Keywords: material extrusion; polymer; melting; heat transfer; finite element analysis; level-set method

1. Introduction

Since the patent of Crump [1], the fused filament fabrication (FFF or FDM™ for Fused Deposition Modeling) does not significantly change in its principle. Nowadays, the market of FFF 3D printers is the majority of additive manufacturing. Due to the low cost of materials and energy, FFF 3D printers are accessible to everyone. Nevertheless, the extension to high-performance polymers needs a better control of the process leading to more expensive printers devoted to industrial purposes.

*Corresponding author: Tel. +33 (4) 93 95 74 34.
Email address: franck.pigeonneau@minesparis.psl.eu (F. Pigeonneau)

Despite the high level of technology, the understanding of a FFF 3D printer is still partial. To print an object, the material is added in a molten state after melting in a hot-end (also called extruder or liquefier) to make a filament of a few hundreds of micrometers in diameter. The way to melt the polymer in the extruder is still debated. Bellini et al. [2], the first to study the melting of the polymer in the liquefier, considered that "the dynamics of the liquefier is one of the most complicated phenomena to analyze in a FDM process".

In general, the melting of polymer is achieved in a block heated by a cartridge completed by a thermistor to control the temperature. A nozzle is consolidated of the heat block. Technical details can be found for instance in the website [3] and will be also presented in § 2. Consequently, the melting is achieved through a channel of a few tens of millimeters in length. For a 1.75 mm diameter filament, the channel has a diameter of 2 mm. Bellini et al. [2] assumed that the polymer is fully melted inside the nozzle with a temperature equal to the melting temperature. The extruder is considered to be filled with polymer. From this simplified model, they determined the pressure drop through the nozzle using a power-law behavior for the molten polymer rheology. Nevertheless, the printer used by Bellini et al. [2] is poorly described compared to the recent printers. For instance, the geometry of the nozzle is not described.

Cited as the reference model by Turner et al. [4], the model of Bellini et al. [2] has been recently called into question by Osswald et al. [5]. These authors claimed that the model of Bellini et al. [2] would be valid only for small flow rates. They argued that in this last situation, the heat diffusion is enough efficient to obtain an uniform temperature as assumed in [2]. When the feeding (inlet) velocity becomes larger than $0.25\,\mathrm{mm\,s^{-1}}$, Osswald et al. [5] proposed a new model of melting. They considered that the melting area is more reduced close to the capillary tube at the end of the nozzle and occurs on the wall of the convergent. Based on this model, the pressure drop is analytically determined using a hydrodynamic model of a Newtonian fluid. The force required to push a filament through an extruder is also experimentally investigated in [5].

Serdeczny et al. [6] provided the first Computational Fluid Dynamics (CFD) study in which the air gap between the interior cylinder of the heat block and the polymer is accounted for. The polymer/air interface is tracked using a Volume-of-fluid method. They observed a rising of the triple line corresponding to the contact line between the two fluids and the interior wall of the extruder. The triple line is stabilized after 50 s when the feeding velocity is $0.67\,\mathrm{mm\,s^{-1}}$. Beside the numerical investigations, Serdeczny et al. [6] developed an experimental set-up to determine the feeding force for various working conditions.

To investigate numerically the melting of a filament, Kattinger et al. [7] described the fluid motion coupled to the heat transfer in the hot-end using a finite volume method. As already mentioned above, an air gap exists between the wall of the extruder and the polymer filament, Kattinger et al. [7] assumed that the filament moves through the extruder with a shear-free condition when the polymer is not in contact with the nozzle. When the polymer reaches the nozzle, the no-slip condition is used. In the numerical model described by Kattinger et al. [7], only the polymer domain is considered. Apart from in the nozzle, the air gap does not change with time. The heat transfer is also taken into account using heat transfer coefficients to account for the radial heating due to the heat block.

In the works [5, 7], the heat transfer is only limited when the polymer is in contact

with the nozzle assuming that the polymer stays with the same morphology through the extruder. The heat transfer described by Bellini et al. [2] or Osswald et al. [5] is purely axial while the heating is provided radially by the heat block. Even if Kattinger et al. [7] take into account the radial heating with the introduction of heat transfer coefficients, it stays limited. Conversely, other contributions consider that the gap between the extruder and the polymer does not exist. Nikzad et al. [8] studied the heating in the extruder of the FDM3000 printer of the Stratasys assuming a perfect contact between the polymer and the extruder. More recently, Pigeonneau et al. [9] developed a numerical model taking into account the shear-thinning of the polymer and the temperature shift using Carreau-Yasuda's law. The generalized Navier-Stokes equations are coupled with the heat transfer through the extruder. The effect of the air gap was investigated using a heat transfer coefficient based on the air thermal resistance model. To agree with the experimental results of Peng et al. [10], Pigeonneau et al. [9] claimed that the contact between the extruder and the polymer should be perfect. Recently, Hong et al. [11] developed a clever experimental set-up to observe the dynamics of the air gap through a transparent tube modeling an extruder. For both PLA and ABS polymers, the air gap is removed due to the introduction of the filament in the tube. Nevertheless, the experiment set-up developed in [11] is far from a real extruder in which the heating is more efficient.

Even if the contribution of Serdeczny et al. [6] is significant, their numerical model is debatable. Under the boundary conditions chosen in [6], the air can not exit the heat block from the top while the air is free to escape. Their numerical simulations show a small gap pocket at the end of the computation near the entrance where the air is under pressure. What is the effect on the dynamics of the contact line? Moreover, the transition of the behavior of the polymer around the glass transition temperature is sharply described in [6]. Below T_g, the polymer behaves like a solid and above T_g the polymer is considered like a fluid with the viscosity described according to a power law. In general, the polymer rheology presents a Newtonian plateau at small shear rates completely absent in [6].

Consequently, the purpose of the current article is to clarify the melting of an amorphous polymer through a liquefier. To address this issue, a numerical method taking into account both the air gap and the polymer is developed. In section 2, the problem statement is detailed with a multiphase flow behavior using a level-set method. The heat transfer is also described. Results and discussion will be then presented in section 3. Section 4 closes the article with a synthesis and perspectives.

2. Problem statement

2.1. Geometry

The extruder V6 designed by E3D is depicted in Figure 1-(a), see [3] for more details. This extruder equips many 3D printers and can be considered as an emblematic example of available extruders in the market. The essential parts of the device are reported in this cut view. The polymer is pushed through the extruder with a guide at the top of the extruder. To prevent the heating in the guide area, a heat sink is added completed by a fan to extract the maximum of heat out of the heat block. Moreover, a small separation, designated as heatbreak, is added between the heat sink and the heat block. The heat

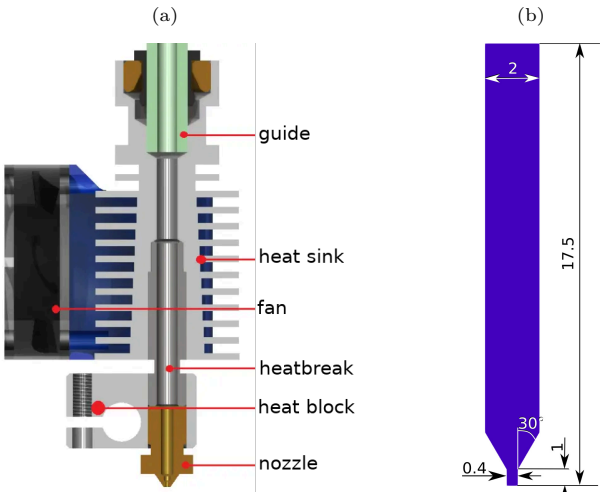

Figure 1: (a) Cut view of the extruder V6 designed by E3D according to [3] and (b) channel with dimensions (given in mm) used in the numerical computation.

block is heated with an electrical cartridge. The control of the temperature is done with a thermistor.

It is assumed that the polymer stays in a solid state until its introduction into the heat block. Consequently, only the channel through which the polymer is melted in the heat block is considered in this present work. By assuming the homogeneity of temperature in the heat block and the nozzle, the problem is reduced to the heat transfer and fluid dynamics through a channel corresponding to the assembling of the heatbreak, the heat block and the nozzle.

Figure 1-(b) is a cut view of the numerical domain used in the following work. According to the design provided in [3], the total length corresponds to the domain heated by the cartridge. The channel in the heat block has a diameter, D, equal to 2 mm. A nozzle with an outlet diameter, d, equal to 0.4 mm and a capillary tube of 1 mm in length is used. The half-angle of the convergent is equal to 30°.

2.2. Balance equations

The two-phase dynamics to track both the air and the polymer phases are described as single-fluid representation [12]. The interface between the two phases is assumed sharp and is implicitly described using a level-set function [13]. Initially, the polymer is partially introduced in the extruder at room temperature, T_0. The surrounding air is assumed to be thermally balanced with the extruder. Consequently, the initial temperature of the air is equal to the extruder temperature, written T_∞. The properties, dynamic viscosity, and thermal conductivity of air are taken from Kadoya et al. [14]. In the first approximation, the physical properties of air are determined at T_∞ and do not change with time. Consequently, the air is assumed incompressible.

The amorphous polymer, characterized by its glass transition temperature T_g, is assumed incompressible. Here, an ABS polymer characterized in [9] is used. The value of T_g is equal to 378.15 K. According to Bird et al. [15, Chap. 4 & 9], the use of a

generalized Newtonian fluid is justified in the fluid domain above T_g. However, as already done by Xia et al. [16] and Pigeonneau et al. [9], the same behavior is considered below the glass transition temperature. The temperature dependence of the viscosity leads to very high values which mimic a solid behavior. The dynamic viscosity is given by Carreau-Yasuda's law [17, 15] as follows

$$\eta_p(\dot{\gamma}, T) = \frac{\eta_{p,0} a_T}{\left[1 + (\lambda a_T \dot{\gamma})^a\right]^{(1-n)/a}}, \tag{1}$$

in which $\eta_{p,0}$ is the Newtonian plateau viscosity of the polymer, n the power law index, λ a time constant depending on the nature of the polymer and a a parameter to describe the transition between the Newtonian plateau and the power-law regime, T the absolute temperature, $\dot{\gamma}$ the generalized shear rate defined by

$$\dot{\gamma} = \sqrt{2\dot{\boldsymbol{\epsilon}} : \dot{\boldsymbol{\epsilon}}}, \tag{2}$$

and $\dot{\boldsymbol{\epsilon}}$ the rate-of-strain tensor given by

$$\dot{\boldsymbol{\epsilon}} = \frac{1}{2}\left(\boldsymbol{\nabla}\boldsymbol{u} + \boldsymbol{\nabla}^t\boldsymbol{u}\right), \tag{3}$$

in which $\boldsymbol{u}$ is the fluid velocity. The symbol ":" in eq. (2) is the double dot product operator defined in [18] and the exponent ^{t} is used for the tensor transposition.

The shift factor a_T follows Arrhenius's law given by

$$a_T = \exp\left[\frac{E_a}{R}\left(\frac{1}{T} - \frac{1}{T_{\text{ref}}}\right)\right], \tag{4}$$

with E_a the activation energy, R the ideal gas constant and T_{ref} a reference temperature. As already pinpointed in [9], the shift factor is approximately equal to $4 \cdot 10^3$ at T_g. In this case, the fluid moves according to a "solid body motion" with a rate-of-strain tensor equal to zero.

As usual, the problem is normalized. The spatial coordinates are reduced by the inlet diameter, D=2 mm. The characteristic velocity is taken as equal to the outlet (or extrusion) velocity

$$U = \frac{4Q}{\pi d^2}, \tag{5}$$

with Q the volumetric flow rate and d the diameter of the capillary tube of the nozzle, equal to 0.4 mm. The dynamic viscosity is scaled with the viscosity $\eta_{p,0}$ of the Newtonian plateau. At first glance, the viscosity forces are larger than the inertial forces. Consequently, the pressure is normalized by $\eta_{p,0}U/D$. The shear rate is also reduced using U/D. Since the range of temperature is between T_0, the inlet temperature, and T_∞ the extruder temperature, the dimensionless temperature is written as follows

$$\theta = \frac{T - T_0}{T_\infty - T_0}. \tag{6}$$

Density and specific heat at constant pressure are normalized by ρ_p, and $C_{p,p}$, respectively.

For convenience, the dimensionless variables are written without a particular symbol. The system of balance equations is then given by

$$\boldsymbol{\nabla}\cdot\boldsymbol{u} = 0, \tag{7}$$

$$\mathrm{Re}\,\rho\frac{D\boldsymbol{u}}{Dt} = -\boldsymbol{\nabla}P + \boldsymbol{\nabla}\cdot[2\eta(\dot\gamma,\theta,\varphi)\dot{\boldsymbol{\epsilon}}] + \mathrm{Ca}^{-1}\,\kappa\|\boldsymbol{\nabla}\varphi\|\delta(\varphi)\boldsymbol{n}_\varphi - \mathrm{Ga}\,\rho\boldsymbol{k}, \tag{8}$$

$$\mathrm{Pe}\,\rho C_p\frac{D\theta}{Dt} = \boldsymbol{\nabla}\cdot[k\boldsymbol{\nabla}\theta] + \mathrm{Br}\,\eta(\dot\gamma,\theta,\varphi)\dot\gamma^2, \tag{9}$$

$$\frac{D\varphi}{Dt} = 0. \tag{10}$$

Equations (7), (8) and (9) correspond to volume, momentum and heat balances, respectively. Recall that due to the discontinuities of physical properties and variables through the polymer/air interface, these equations must be taken in the meaning of the distribution theory [19] or [20, Chap. 20]. The polymer/air interface is assumed without mass meaning that its Lebesgue measure is equal to zero. Equation (10) describes the transport of the level-set function, φ, without source term. In a such case, the polymer/air interface is simply a material surface.

Due to the normalization of the momentum equation by the viscous stress, the inertia term is proportional to the Reynolds number, Re. Apart from the two first terms on the right-hand side of (8) corresponding to the pressure and viscous stresses, the third term is the contribution of the surface tension. This stress results from the jump condition at the fluid interface [21, 12]. This term is inversely proportional to the capillary number, Ca. The symbol $\delta(\varphi)$ is the Dirac distribution function. The vector $\boldsymbol{n}_\varphi$ is the unit normal vector at the interface defined by

$$\boldsymbol{n}_\varphi = \frac{\boldsymbol{\nabla}\varphi}{\|\boldsymbol{\nabla}\varphi\|}, \tag{11}$$

and κ is the mean curvature given by [22]:

$$\kappa = -\boldsymbol{\nabla}_S\cdot\boldsymbol{n}_\varphi. \tag{12}$$

The last term of the right-hand side of (8) is due to the gravity force directed downward with $\boldsymbol{k}$ the unit vector in the z-axis direction. The gravity force is proportional to the Galilei number, Ga, that is the ratio of the gravity to the viscous force. In eq. (9), the effect of the pressure work has been neglected due to the low compressibility of the polymer and the air. The last term of the right-hand side of (9) is the heating source due to the viscous dissipation characterized by the Brinkman number, Br.

All properties are defined as a function of characteristic functions of each phase. If the level-set function is defined as positive in the polymer phase, the density is then written as follows

$$\rho(\varphi) = H(\varphi) + \rho_{\mathrm{air}}\left[1 - H(\varphi)\right], \tag{13}$$

with $H(\varphi)$ the Heaviside distribution function. The density of air is normalized by the polymer density. The same relation of (13) is used to determine the dynamic viscosity, η, the heat capacity at constant pressure, C_p and thermal conductivity k. Finally, recall the dimensionless form the dynamic viscosity of the polymer is given by [9]

$$\eta_p(\dot\gamma,\theta) = \frac{a_T}{\left[1 + (\mathrm{Wi}\,a_T\dot\gamma)^a\right]^{(1-n)/a}}, \tag{14}$$

Table 1: Dimensionless numbers, names, definitions and typical values obtained for an extrusion velocity of $3\,\mathrm{m\,min^{-1}}$.

Reynolds	capillary	Galilei	Péclet	Brinkman	Weissenberg
Re	Ca	Ga	Pe	Br	Wi
$\frac{\rho_p U D}{\eta_{p,0}}$	$\frac{U\eta_{p,0}}{\gamma}$	$\frac{\rho_p g D^2}{U\eta_{p,0}}$	$\frac{UD}{a_p}$	$\frac{\eta_{p,0}U^2}{k_p(T_\infty - T_0)}$	$\frac{\lambda U}{D}$
3.8×10^{-5}	5×10^{3}	2.9×10^{-4}	1.15×10^{3}	1.7×10^{-1}	8×10^{-1}

with Wi is a Weissenberg number defined in Table 1.

Dimensionless numbers are listed in Table 1 with name and definition. Apart from U, D, $\eta_{p,0}$ and λ already defined above, ρ_p is the polymer density, γ the surface tension between the two phases, g the acceleration of the gravity, k_p the thermal conductivity of the polymer and $a_p = k_p/(\rho_p C_{p,p})$ the thermal diffusivity of the polymer. With the numerical values of physical properties and with an outlet velocity taken equal to $3\,\mathrm{m\,min^{-1}}$, the values of each dimensionless number are reported in Table 1. As expected, the Reynolds number is less than one meaning that the inertia is negligible. Nevertheless, the inertia term will be conserved in the numerical implementation because, in the air domain, the typical Reynolds number can be more significant. The capillary number is high enough to mention that the capillary effect will be weak as for the gravity force, small Galilei number. The large value of the Péclet number means that the advection plays an important role in the heat transfer through the channel. The self-heating of the polymer should be moderated due to the weak value of the Brinkman number.

2.3. Initial and boundary conditions

Before solving numerically the system of equations (7-10), initial and boundary conditions have to be pointed out. Figure 2 provides the initial state with the polymer partially immersed in the extruder. The filament diameter is equal to d_{fil}=1.75 mm. Around the polymer, the channel is filled with air in blue. The temperature of the polymer is equal to the room temperature which is equal to θ=0 under the dimensionless form. The temperature of the air is assumed to be equal to the extruder temperature, i.e. θ=1. Initially, both polymer and air are at rest.

In Figure 2, the main boundary conditions are also reported. The values reported in Figure 2 are written in dimensionless form. The entrance section, at the top of the domain, is decomposed in two sections, $\partial\Omega_{\mathrm{in}}$ and $\partial\Omega_{\mathrm{gas}}$. On $\partial\Omega_{\mathrm{in}}$, the boundary conditions on the polymer are written on the top left of Figure 2. The velocity is set equal to the feeding velocity of the polymer over the area corresponding to the filament. Due to the mass conservation, the normalized magnitude of feeding velocity is simply given by the d/d_{fil} ratio squared. Temperature is set equal to room temperature and the level-set function is defined as positive at the input to establish the iso-value φ=0 at the polymer/air interface at any time. On the free polymer crown, at the top of the channel, written on the top right of Figure 2 and designated by $\partial\Omega_{\mathrm{gas}}$, the Cauchy stress normal is assumed to be free meaning that the pressure is equal to zero. This is the major difference with the condition used by Serdeczny et al. [6] for which the air can not escape freely from the extruder. Thermal flux and the level-set flux are equal to zero. On the channel wall, $\partial\Omega_{\mathrm{w}}$, the boundary conditions are written on the left of Figure 2. No-slip condition is used for the velocity. Temperature is equal to the extruder

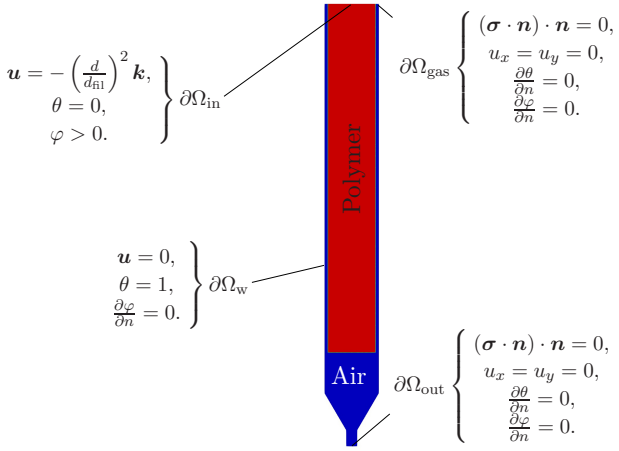

Figure 2: Boundary conditions on the channel written in a dimensionless form with the initial position of the polymer and air with $\boldsymbol{n}$ the outward unit normal to the boundary of the domain.

temperature equal to one in dimensionless form. This condition is fully justified since the thermal effusivity of the heat block in aluminum is 33 times larger than the polymer effusivity and 4452 times larger than the effusivity of air. For the level-set function, no flux condition is used. This means that at the wall, the contact angle at the triple line is set equal to $\pi/2$. Finally, the outlet conditions are depicted on the bottom right of Figure 2, boundary $\partial\Omega_{\text{out}}$.

Note that numerically, a 3D case is solved. Due to the revolution symmetry, only one-quarter of the domain is considered. This means that apart from the previous boundary conditions, symmetric conditions have to be applied to the two symmetric planes.

2.4. Numerical method

To solve numerically the system of equations (7-10), a time-marching method is used. To determine the temporal derivatives of $\boldsymbol{u}$, θ and φ, a first-order finite-difference method is employed. To ensure numerical stability, an implicit Euler scheme is implemented. The spatial discretization is performed by a finite-element method. The domain is meshed with linear tetrahedral elements. For the Navier-Stokes equations, the discrete $\inf-\sup$ condition is satisfied by using the $\mathbb{P}_1-\text{bubble}/\mathbb{P}_1$ element [23]. The transport equations for the temperature and the level-set function are stabilized by a Streamline Upwind/Petrov-Galerkin method [24]. To catch the polymer/air interface as accurately as possible, an adaptive anisotropic mesh is used and detailed in [25].

As it is well known, the transport of the level-set leads to a loss of the Eikonal property of φ, i.e., $\|\boldsymbol{\nabla}\varphi\| \neq 1$. A direct reinitialization method is used. This technique works in three steps: (i) the interface corresponding to the zero iso-value of the level-set function is discretized into a collection of simple elements; (ii) the distance is then calculated for each node to all elements of the domain and (iii) the smallest one is stored becoming the updated value of the level-set function, see [26] for more details. This method is applied every two-time steps.

Table 2: Parameters used in Carreau-Yasuda and Arrhenius laws for the acrylonitrile butadiene styrene.

$\eta_{p,0}$	λ	n	a	E_a	T_{ref}
Pa s	s	–	–	kJ mol^{-1}	K
3.04×10^3	3.2×10^{-2}	0.28	0.6	115.06	493.15

Table 3: Thermal properties for the acrylonitrile butadiene styrene from [28] and air from [14].

ρ	C_p	k
kg/m^3	J kg^{-1} K^{-1}	W m^{-1} K^{-1}
ABS		
1150	2100	0.21
Air, $T = T_{\text{ext}}$		
0.701	1034.78	0.0399

Numerically, the Heaviside and Dirac functions have to be regularized according to functions defined by [27]:

$$H_\varepsilon(\varphi) = \begin{cases} 0 & \text{if } \varphi < -\varepsilon; \\ \frac{1}{2}\left[1 + \frac{\varphi}{\varepsilon} + \frac{1}{\pi}\sin\left(\pi\frac{\varphi}{\varepsilon}\right)\right] & \text{if } |\varphi| \leq \varepsilon; \\ 1 & \text{if } \varphi > \varepsilon, \end{cases} \tag{15}$$

and

$$\delta_\varepsilon(\varphi) = \frac{dH_\varepsilon(\varphi)}{d\varphi}. \tag{16}$$

The numerical parameter ε is chosen to be equal to a distance of a few of minimal mesh sizes, $h_{\min}$. A factor of three or five of $h_{\min}$ gives an acceptable regularization of the properties. Numerical computations have been done with $h_{\min}$ equal to 10^{-3}.

3. Results and discussion

The numerical computations are carried out using an acrylonitrile butadiene styrene (ABS) polymer already characterized in [9]. The parameters for determining the dynamic viscosity of the ABS polymer and the shift factor are gathered in Table 2. The thermal properties of the ABS polymer taken from [28] and of the air according to [14] are summarized in Table 3. According to Bellehumeur et al. [29], the surface tension required to determine the capillary number is taken equal to 2.8×10^{-2} N m^{-1}.

The working conditions chosen for numerical computations are given in Table 4. Mainly, three values of extrusion velocity are tested. The feeding velocity, U_{in} is also indicated. The smallest U is higher than the velocity mentioned by Osswald et al. [5]. Nevertheless, the feeding velocity remains small enough for the typical values used in the applications.

3.1. Transitional regime

The first stage is only a transport of the filament polymer until the contact with the nozzle. The polymer moves simply with a plug flow heated up by the warm surrounding

Table 4: Data of working conditions.

Case	U (m min^{-1})	U_{in} (mm s^{-1})	T_0 (K)	T_∞ (K)
1	1	8.71×10^{-1}		
2	3	2.61	297.15	503.15
3	6	5.22		

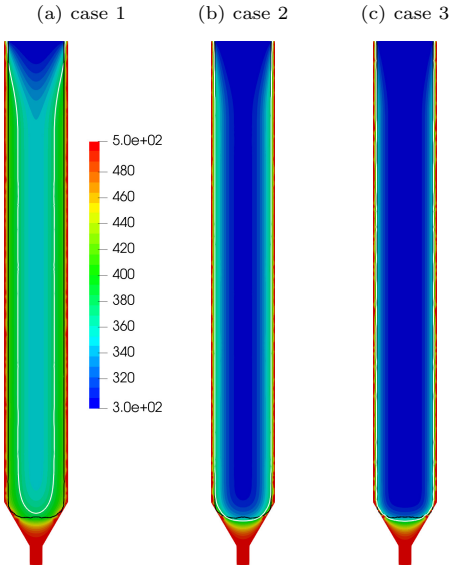

Figure 3: Temperature field (in K) for (a) case 1, (b) case 2, and (c) case 3 of Table 4 when the normalized time is equal to 18 corresponding to 2.16 s, 0.72 s and 0.36 s for cases 1, 2 and 3 respectively.

air. Figure 3 depicts the temperature field in K when the polymer is just in contact with the nozzle for the three cases listed in Table 4. Under a dimensionless formulation, the contact appears at the same time for the three cases, i.e. for t=18. This duration corresponds to 2.16 s, 0.72 s and 0.36 s for cases 1, 2 and 3 respectively. The level set position equal to zero corresponding to the polymer/air interface is represented in solid black line. The solid white line represents the iso-T_g of the polymer. In case 1, the time required to have contact is sufficiently large to heat up radially the polymer over a significant length. A large part of the polymer is already heated above T_g. Only the area close to the inlet stays cool. For the two other cases, the temperature field underlines that the thermal conduction is less efficient. The polymer is close to the initial temperature. The locations of the interface and the iso-T_g are very close.

In Figure 4, the temperature field in K, the polymer/air interface and the iso-T_g are given for t starting from 3 s and increasing by a time step of 3 s until t=18 s for the case 1. At t=3 s in Figure 4-(a), the polymer is in contact with the extruder just above the conical part until the exit of the extruder. The axial coordinate of the contact line, z_{cl}, has been reported in Figure 4-(a). The contact between the polymer with the extruder enhances the heat transfer since the polymer exhibits a temperature close to the extruder temperature. The triple line rises up along the interior of the extruder. When t=12 s,

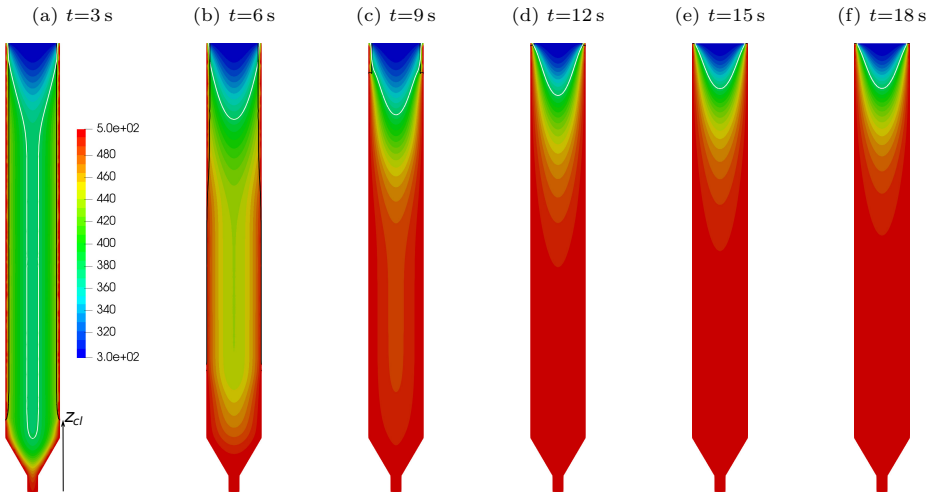

Figure 4: Temperature field (in K) for case 1 for various increasing time starting at t=3 s with a time step of 3 s until t=18 s. The vertical position of the contact line, z_{cl}, has been reported for t=3 s.

the air gap has completely disappeared. Figure 4-(e) and Figure 4-(f) are very similar suggesting that the steady-state regime is reached. The air gap is then removed after a physical time around 15 s when the extrusion velocity is equal to $1\,\mathrm{m\,min^{-1}}$. This time is the same order of magnitude as the prediction of Serdeczny et al. [6]. With increasing time, the iso-T_g is more and more localized close to the inlet of the extruder. In these conditions, the temperature is uniform in a large portion of the extruder. The view proposed by Bellini et al. [2] is then valid even for this case for which the feeding velocity is larger than $0.25\,\mathrm{mm\,s^{-1}}$ given as a threshold by Osswald et al. [5].

Figure 5 provides the temperature field, the polymer/air interface and iso-T_g for the case 2 for which the extrusion velocity is multiplied by a factor of three and for t from 1 s to 7 s. The heat transfer changes strongly to the previous case. At a short time, Figure 5-(a), the melting of the polymer occurs mainly from the contact with the extruder. The polymer filament stays at a temperature below T_g practically until contact with the convergent of the nozzle. Only, a thin layer is melted. For t=2 s, the iso-T_g is yet close to the capillary tube of the nozzle. This state is the view proposed by Osswald et al. [5]. But, the state is unsteady. With time, the polymer is more and more heated up. This dynamics is strongly coupled to the motion of the contact line. The triple line rises up until t=5 s. As seen in Figure 5-(f) and (g), the contact line does not move. This means that an air gap is not fully removed for case 2. This state has been observed in [6]. Nevertheless, in our numerical model, the air is free to escape meaning that the solution found here is the solution to the dynamics of the two-phase flows. This suggests that the polymer enters in the heat block without contact over a non-negligible length. This air gap plays the role of a thermal insulator as shown in Figure 5-(g) in which the iso-T_g is quasi vertical over a length corresponding to the air gap.

Figure 6 presents for a time starting from 1 s to 4 s the temperature field, the polymer/air interface and iso-T_g for an extrusion velocity equal to $6\,\mathrm{m\,min^{-1}}$. The advection of the polymer becomes high enough to observe a large area in which the polymer stays

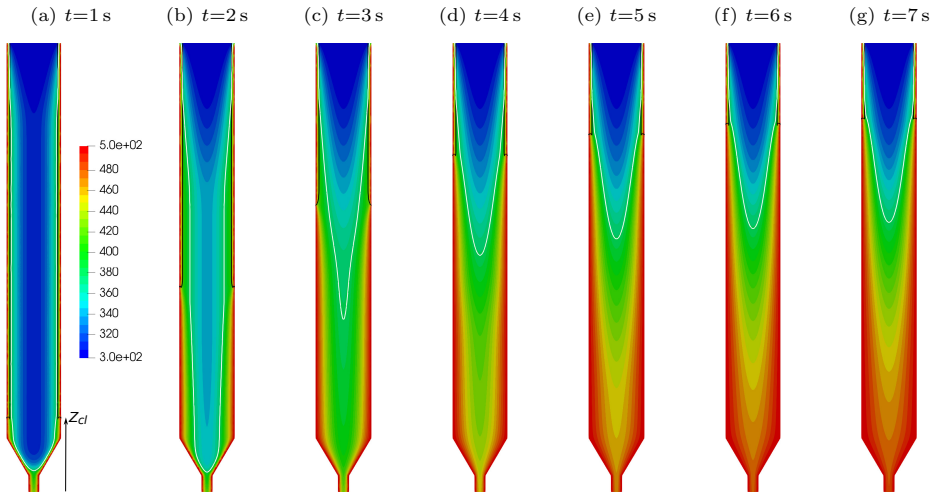

Figure 5: Temperature field (in K) for case 2 for various increasing time starting at t=1 s with a time step of 1 s until t=7 s. The vertical position of the contact line, z_{cl}, has been reported for t=1 s.

cold. A singular behavior of case 3 is due to the air gap. In a first stage, the air gap disappears quasi completely at t=10 s (Figure 6-(c)) to reappear for longer times (Figure 6-(d-g)). At the same time, the iso-T_g extending until the exit of the nozzle at a short time becomes shorter and shorter with the time. Note that the temperature is far from uniform at the exit of the nozzle.

To see the dynamics of the contact line, the vertical position of this line in the tube z_{cl} is plotted in Figure 7 as a function of time given in physical dimensions. For case 1, i.e. U=1 m min^{-1}, after a delay corresponding to the time needed for the polymer to move freely in the nozzle, the triple line rises up approximately linearly with time. After 15 s, the triple line reaches the top of the heat block. When the extrusion velocity is equal to 3 m min^{-1}, the triple line rises up to reach a stationary position after 15 s. As already pinpointed above, the dynamics for case 3, i.e. U=6 m min^{-1}, is not monotone with time. The triple line rises up until the top of the extruder. The air gap is slowly created to reach a stationary state after a duration around 14 s.

Even if our conditions are more ideal than to those of Hong et al. [11], the overall dynamics obtained numerically is in agreement with the experimental observations. The presence of the air gap at the beginning of the extruder for a large feeding velocity is also experimentally observed.

3.2. Steady-state regime

The temperature fields for the three cases obtained in the steady-state regime are depicted in Figure 8. In case 1, the temperature appears quasi uniform in a large part of the extruder. This means that the radial heating by the heat block is efficient. This picture is close to the description drawn by Bellini et al. [2]. For the second case, Figure 8-(b), the influence of the transport by convection is stronger than for the case 1. A cold core with a temperature close to the inlet temperature is present over a large distance. The influence of the advection is more pronounced in the last case, Figure 8-(c).

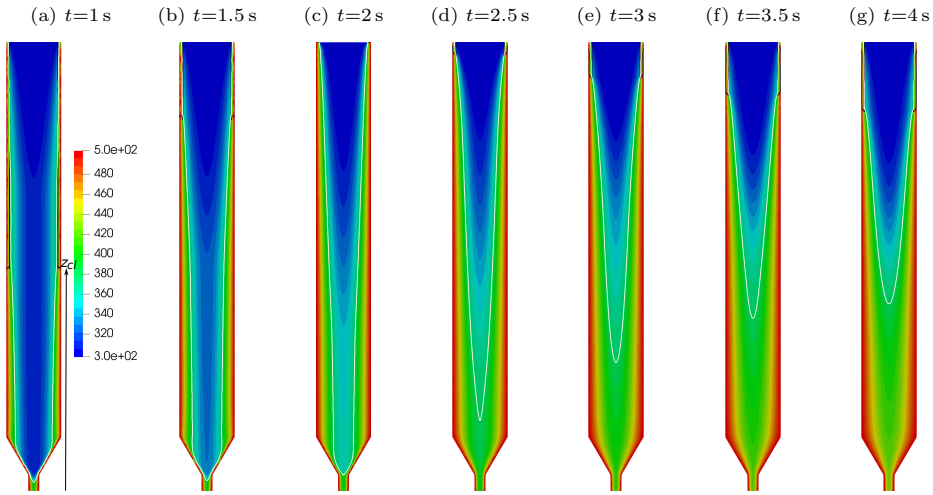

Figure 6: Temperature field (in K) for case 3 for various increasing time starting at t=1 s with a time step of 0.5 s until t=4 s. The vertical position of the contact line, z_{cl}, has been reported for t=5 s.

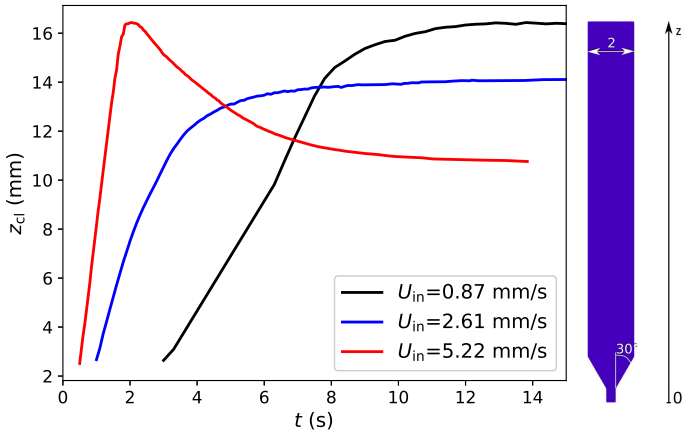

Figure 7: Behavior of the contact line (z_{cl}) as a function of time t (s) for the three velocities.

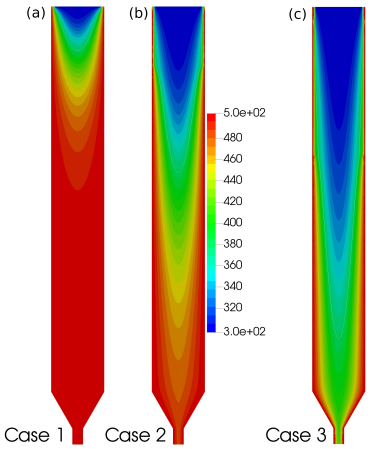

Figure 8: Temperature field (in K) in a symmetric plane for the three velocities: (a) U=1 m min^{-1}, (b) U=3 m min^{-1} and (c) U=6 m min^{-1}.

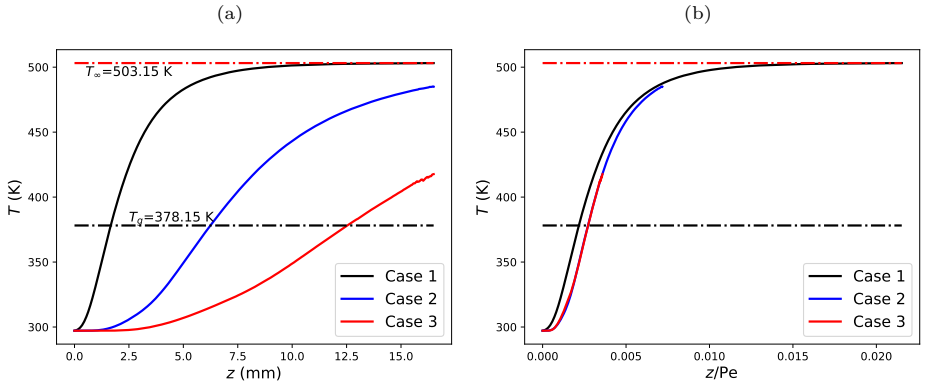

Figure 9: Behavior of the temperature (K) along the symmetry axis as a function of : (a) the height in the nozzle z (mm) and (b) $z/\,\mathrm{Pe}$ for the three cases.

Only the polymer in contact with the extruder is heated up at the heating temperature. The core of the filament stays relatively cold.

Figure 9-(a) depicts the temperature in K in the axial position as a function of the longitudinal position given in mm. Both the glass transition temperature of the ABS and the extruder temperature have been reported. At the lowest velocity (case 1), the heating is high enough to observe that the axial temperature reaches the extruder temperature. When the feeding velocity is multiplied by 3, the axial temperature never reaches the extruder temperature. The worst situation is observed for the last case. The heating of a fluid has been studied by many authors. Bejan [30, Sec. 3.5] synthesized the heat transfer in a developing flow through a channel, the so-called Graetz problem.

It is expected that the temperature is self-similar when it is given as a function of $z/\,\mathrm{Pe}$ with z already normalized by the duct diameter. Figure 9-(b) represents the temperature as a function of $z/\,\mathrm{Pe}$ for the three cases. The Péclet numbers are equal 383.33, 1150

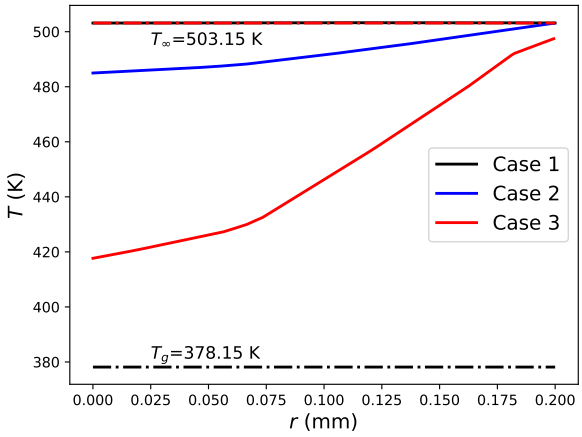

Figure 10: Temperature (K) along a radial axis r (mm) for the three cases at the nozzle exit.

and 2300 respectively for cases 1, 2, and 3. The self-similarity is well observed for the two last cases. For the first case, the increase of the temperature is stiffer than the two other cases. It is mainly due to the total absence of an air gap for the case 1. For the two other cases, the temperature profile presents a sigmoidal profile.

Figure 10 gives the radial profiles of the temperature in the nozzle exit. As expected, the thermal gradient increases with the extrusion velocity. While for the case 1, the temperature is uniformly equal to the extruder temperature over the radial position, a thermal gradient increases for the second case. In the last situation, with U=6 m min^{-1}, the thermal difference is around 70 K.

3.3. Feeding force

As already analyzed in [5, 6], the feeding force needed to push the polymer filament is a relevant quantity to determine. To get numerically this quantity, the surface force of the Cauchy stress on the wall of the extruder, boundary $\partial\Omega_{\mathrm{w}}$ in Figure 2, has to be integrated over the total boundary $\partial\Omega_{\mathrm{w}}$. To avoid the determination of the Cauchy stress, a significant result of fluid mechanics is used. According to Berker [31], the tension on a wall with the no-slip condition and for an incompressible fluid is given by

$$\boldsymbol{T} = P\boldsymbol{n} + 2\eta\boldsymbol{n} \times \boldsymbol{\omega}, \tag{17}$$

with

$$\boldsymbol{\omega} = \frac{1}{2}\boldsymbol{\nabla} \times \boldsymbol{u}, \tag{18}$$

the vorticity and $\boldsymbol{n}$ the outward unit normal to the boundary $\partial\Omega_{\mathrm{w}}$. The expression of Berker [31] is useful since only the vorticity is needed to compute the tension on the wall. This result is simply a corollary of the Stokes theorem. The vorticity is determined using the software Paraview in post-treatment.

The surface integration of (17) over the boundary $\partial\Omega_{\mathrm{w}}$ gives access to the force required to introduce the filament through the extruder. Figure 11 presents the vertical component of the feeding force in Newton as a function of time (s) for the three cases.

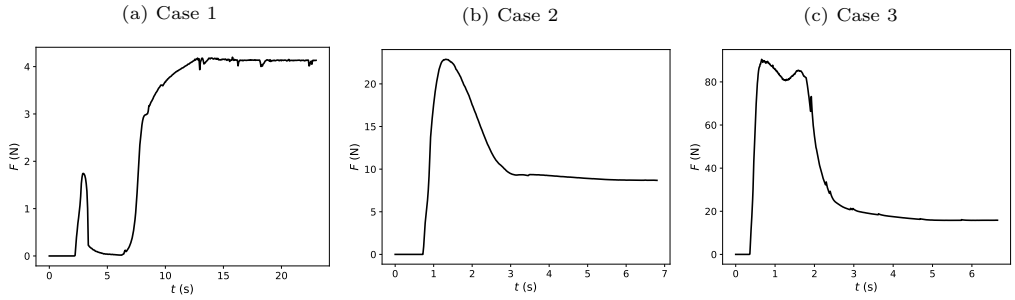

Figure 11: Feeding force (N) as a function of time for the three cases.

For case 1, Figure 11-(a), the force is quasi-equal to zero at the beginning. A sudden increase is observed at t=2.5 s when the polymer becomes in contact with the nozzle. After a decrease, the force increases to reach a plateau for which the value of the feeding force is around 4 N.

For the case 2, Figure 11-(b), the force increases sharply from t=0.8 s to reach a maximum of 22 N at t=1.5 s. This significant force comes from the high value of the viscosity due to the temperature is under T_g at short times. Finally, with the heating of the polymer, the force needed to push the filament decreases to reach a value around 9 N. Case 3 exhibits a similar behavior apart from the amplitude of the force which is larger than 80 N. Even if the steady-state force can be acceptable for the feeding mechanism, the transient stage could produce jamming. Apart from case 1, for which the steady-state regimes on the triple line and the feeding force are observed approximately at the same time, the two other cases behave differently. While the stationary position of the triple line required a few tens of seconds to be observed, the feeding force reaches a plateau over a time around 5 s.

For comparison with experimental data, the results provided by Serdeczny et al. [6] are used by selecting the closest temperature to our conditions. In Figure 12, the feeding force is plotted as a function of the feeding velocity, U_{in}. The black dots correspond to our numerical solution obtained with an extruder temperature equal to 503.15 K. The blue crosses are the experimental data obtained by Serdeczny et al. [6] on the same extruder as our numerical simulations with an equivalent polymer and for an extruder temperature equal to 498.15 K. The numerical force is very close to the experimental data for the two lowest feeding velocities. The numerical simulation underestimates the feeding force for the highest velocity used. From the numerical simulations, the feeding force appears to be linear with the feeding velocity, whereas the experimental data show a non-linear behavior. Although the experimental predictions present large uncertainties at high feeding velocity (not represented in Figure 12), this disagreement has to be understood.

4. Synthesis and perspectives

This work has been devoted to numerical investigations of the melting of a polymer inside an extruder (type E3D-V6). A multiphase model considers the two fluids (air and polymer) as a single material. The level-set method describes implicitly the interface

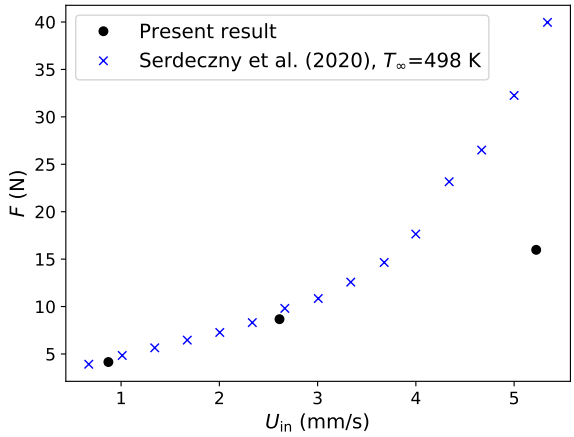

Figure 12: feeding force ,F (N), as a function of U_{in} (mm s^{-1}) of the present study for T_∞=503.15 K and comparison with experimental data of Serdeczny et al. [6] obtained at T_∞=498.15 K.

between the two fluids. To accurately capture the interface and the thermal behavior, an adaptive mesh refinement is also implemented. By this way, it is possible to accurately describe the first steps of the melting of the filament through the extruder. At very short times, the melting is localized near the contact with the nozzle. These results are in agreement with the previous conclusions of Osswald et al. [5]. However, the polymer rises up along the nozzle wall and the heat block leading to a reduction of the air gap. At low velocities, the air gap can disappear. The increase of the extrusion velocity (or feeding velocity) leads to the occurrence of the air gap at the top of the extruder. This air layer is an efficient thermal insulator leading to the extinction of an area of polymer with a temperature below the glass transition temperature. The rising of the air gap and the establishment of the thermal balance take a few tens of seconds. This transitional regime needs a time not negligible in comparison to the time required to deposit a thread of a few of centimeters.

The creation of an air gap confirms the previous predictions of Serdeczny et al. [6]. In our numerical model, the air gap is free to form or not. The occurrence of the air gap when the feeding velocity is larger than 0.87 mm s^{-1} limits the heat transfer between the heat block and the polymer. In such a situation, the model proposed by Osswald et al. [5] seems appropriate. In the first stage, the melting of the polymer occurs close to the wall of the extruder.

The determination of the feeding force gives an acceptable agreement with the experimental data. This integral result allows relying on the numerical model developed for this work. Notwithstanding the novelty of our numerical simulations, many improvements have been done. The polymer has been considered as a pseudoplastic fluid. To take into account the elastic contribution, a viscoelastic fluid behavior would be required with a non-linear law to take into account the shear thinning effect. The presence of the triple line is a significant issue to address due to the singularity of the shear rate at the triple line. Apart from these new numerical investigations, experiences could be also developed to see through an extruder using an X-ray source on a synchrotron facility.

Acknowledgements

This research is supported by the Carnot Institutes M.I.N.E.S and ingenierie@Lyon through the CARATS project funded by the Programme des Investissements d'Avenir and the Agence Nationale de la Recherche.

Credit author statement

S. Marion: Investigation, Methodology, Validation, Formal analysis, Software, Writing - Review & Editing. **L. Sardo**: Software, Methodology, Writing - Review & Editing. **T. Joffre**: Conceptualisation, Formal analysis, Methodology, Writing - Review & Editing. **F. Pigeonneau**: Conceptualisation, Investigation, Methodology, Validation, Formal analysis, Software, Writing - Original Draft, Supervision.

Declaration of Competing Interest

The authors declare that they have no known competing financial interests or personal relationships that could have appeared to influence the work reported in this article.

References

[1] S. S. Crump, inventor. Stratasys, Inc. Apparatus and method for creating three-dimensional objects. *US patent 5,121,329 A*. 1989.

[2] A. Bellini, S. Güçeri, and M. Bertoldi. Liquefier dynamics in fused deposition. *J. Manuf. Sci. Eng.*, 126(2):237–246, 2004.

[3] E3D-online. E3d help centre. https://e3d-online.zendesk.com/hc/en-us, 2021.

[4] B. N. Turner, R. Strong, and S. A. Gold. A review of melt extrusion additive manufacturing processes: I. Process design and modeling. *Rapid Prototyping J.*, 20(3):192–204, 2014.

[5] T. A. Osswald, J. Puentes, and J. Kattinger. Fused filament fabrication melting model. *Addit. Manuf.*, 22:51–59, 2018.

[6] M. P. Serdeczny, R. Comminal, M. T. Mollah, D. B. Pedersen, and J. Spangenberg. Numerical modeling of the polymer flow through the hot-end in filament-based material extrusion additive manufacturing. *Addit. Manuf.*, 36:101454, 2020.

[7] J. Kattinger, T. Ebinger, R. Kurz, and C. Bonten. Numerical simulation of the complex flow during material extrusion in fused filament fabrication. *Addit. Manuf.*, page 102476, 2021.

[8] M. Nikzad, M. S. Hasan, I. Sbarski, and A. Groth. A study of melt flow analysis of an abs-iron composite in fused deposition modelling process. *Tsinghua Sci. Technol.*, 14(S1):29–37, 2009.

[9] F. Pigeonneau, D. Xu, M. Vincent, and J.-F. Agassant. Heating and flow computations of an amorphous polymer in the liquefier of a material extrusion 3d printer. *Addit. Manuf.*, 32:101001, 2020.

[10] F. Peng, B. D. Vogt, and M. Cakmak. Complex flow and temperature history during melt extrusion in material extrusion additive manufacturing. *Addit. Manuf.*, 22:197 – 206, 2018.

[11] Y. Hong, M. Mrinal, H. S. Phan, V. D. Tran, X. Liu, and C. Luo. In-situ observation of the extrusion processes of acrylonitrile butadiene styrene and polylactic acid for material extrusion additive manufacturing. *Addit. Manuf.*, 49:102507, 2022.

[12] I. Kataoka. Local instant formulation of two-phase flow. *Int. J. Multiphase flow*, 12(5):745–758, 1986.

[13] J. A. Sethian. *Level set methods and fast marching methods. Evolving interfaces in computational geometry, fluid mechanics, computer vision, and materials science.* Cambridge University Press, Cambridge, 1999.

[14] K. Kadoya, N. Matsunaga, and A. Nagashima. Viscosity and thermal conductivity of dry air in the gaseous phase. *J. Phys. Chem. Ref. Data*, 14(4):947–970, 1985.

[15] R. B. Bird, R. C. Armstrong, and O. Hassager. *Dynamics of polymeric liquids: Vol. 1 Fluid mechanics*. Wiley-Interscience, 2nd edition, 1987.
[16] H. Xia, J. Lu, S. Dabiri, and G. Tryggvason. Fully resolved numerical simulations of fused deposition modeling. Part I: Fluid flow. *Rapid Prototyping J.*, 24(2):463–476, 2018.
[17] P. J. Carreau. Rheological equations from molecular network theories. *Trans. Soc. Rheol.*, 16(1):99–127, 1972.
[18] R. B. Bird, W. E. Stewart, and E. N. Lightfoot. *Transport phenomena*. John Wiley and sons, New York, second edition, 2002.
[19] L. Schwartz. *Méthodes Mathématiques pour les Sciences Physiques*. Hermann, Paris, 1961.
[20] A. Prosperetti. *Advanced Mathematics for Applications*. Cambridge Univ Press, Cambridge, 2011.
[21] J.-M. Delhaye. Jump condition and entropy sources in two-phase systems. local instants formulation. *Int. J. Multiphase Flow*, 1:395–409, 1974.
[22] M. E. Gurtin, J. Weissmüller, and F. Larché. A general theory of curved deformable interfaces in solids at equilibrium. *Philos. Mag. A*, 78(5):1093–1109, 1998.
[23] A. Ern and J.-L. Guermond. *Theory and practice of finite elements*, volume 159. Springer Science & Business Media, 2004.
[24] A. N. Brooks and T. J. R. Hughes. Streamline upwind/petrov-galerkin formulations for convection dominated flows with particular emphasis on the incompressible navier-stokes equations. *Comput. Methods Appl. Mech. Engrg.*, 32(1):199–259, 1982.
[25] G. Jannoun, E. Hachem, J. Veysset, and T. Coupez. Anisotropic meshing with time-stepping control for unsteady convection-dominated problems. *Appl. Math. Modell.*, 39(7):1899 – 1916, 2015.
[26] M. Shakoor, B. Scholtes, P.-O. Bouchard, and M. Bernacki. An efficient and parallel level set reinitialization method - application to micromechanics and microstructural evolutions. *Appl. Math. Modell.*, 39(23):7291–7302, 2015.
[27] J. A. Sethian and P. Smereka. Level set methods for fluid interfaces. *Annu. Rev. Fluid Mech.*, 35:341–371, 2003.
[28] M. E. Mackay, Z. R. Swain, C. R. Banbury, D. D. Phan, and D. A. Edwards. The performance of the hot end in a plasticating 3D printer. *J. Rheol.*, 61(2):229–236, 2017.
[29] C. Bellehumeur, L. Li, Q. Sun, and P. Gu. Modeling of bond formation between polymer filaments in the fused deposition modeling process. *J. Manuf. Processes*, 6(2):170–178, 2004.
[30] A. Bejan. *Convection heat transfer*. John Wiley & Sons, 2013.
[31] R. Berker. Intégration des équations du mouvement d'un fluide visqueux incompressible. In *Handbuch der Physik*. Springer, Berlin, 1963.